A new mouse model of thrombopoietin deficiency arising from a spontaneous single base pair mutation.

Platelets

ISSN: 0953-7104 (Print) 1369-1635 (Online) Journal homepage: www.tandfonline.com/journals/iplt20

A new mouse model of thrombopoietin deficiency arising from a spontaneous single base pair mutation

Nan Sophia Han, Emma E. Yvanovich, Shenglin Mei, Harvey G. Roweth, Elisabeth M. Battinelli, David B. Sykes & Ninib Baryawno

To cite this article: Nan Sophia Han, Emma E. Yvanovich, Shenglin Mei, Harvey G. Roweth, Elisabeth M. Battinelli, David B. Sykes & Ninib Baryawno (2026) A new mouse model of thrombopoietin deficiency arising from a spontaneous single base pair mutation, Platelets, 37:1, 2602721, DOI: 10.1080/09537104.2025.2602721

To link to this article: https://doi.org/10.1080/09537104.2025.2602721

PLATELETS
2026, VOL. 37, NO. 1, 2602721
https://doi.org/10.1080/09537104.2025.2602721

Taylor & Francis
Taylor & Francis Group

RESEARCH ARTICLE

OPEN ACCESS Check for updates

A new mouse model of thrombopoietin deficiency arising from a spontaneous single base pair mutation

Nan Sophia Han[a,b], Emma E. Yvanovich[b], Shenglin Mei[c,d], Harvey G. Roweth[e,f,g], Elisabeth M. Battinelli[e,f], David B. Sykes[b,f,h], and Ninib Baryawno[a]

[a]Division of Pediatric Oncology and Pediatric Surgery, Department of Women's and Children's Health, Karolinska Institutet, Stockholm, Sweden; [b]Center for Regenerative Medicine, Massachusetts General Hospital, Boston, MA, USA; [c]Fralin Biomedical Research Institute, Virginia Tech FBRI Cancer Research Center, Washington, DC, USA; [d]Department of Biomedical Sciences and Pathobiology, College of Veterinary Medicine, Virginia Tech, Blacksburg, VA, USA; [e]Division of Hematology, Department of Medicine, Brigham and Women's Hospital, Boston, MA, USA; [f]Harvard Medical School, Boston, MA, USA; [g]School of Biological Sciences, University of Reading, Reading, UK; [h]Division of Hematology, Massachusetts General Hospital Cancer Center, Boston, MA, USA

ABSTRACT

Thrombopoietin (TPO) is the principal regulator of bone marrow platelet production and plays an important role in maintaining hematopoietic stem and progenitor cells. Predominantly produced in the liver, circulating TPO levels are primarily modulated through receptor-mediated clearance of TPO by target cells such as platelets. However, there is an additional component of TPO regulation at the transcriptional level, which may be affected in the setting of platelet-associated diseases. Current TPO knockout mouse models partially limit the study of transcriptional regulation because of disruption of the TPO genomic locus. Here, we describe a novel mouse model of TPO deficiency arising from a spontaneous mutation in a single base pair within exon 5 of the TPO gene. The resulting amino acid change (leucine to histidine at position 121) predicts a dramatic alteration in protein structure, ultimately resulting in a ~ 95% decrease of circulating TPO. The hematological phenotype of this new *C57Bl/6(IMPC)J-TPO^{L121H}* strain mimics that of other mouse models of TPO deficiency, but the genomic locus remains intact and therefore preserves normal TPO transcriptional regulation. We characterize the hematological phenotype of this new strain and discuss its applications as a model of transcriptional TPO regulation and clinical thrombocytopenia. Our findings highlight the theoretical possibility that TPO protein destabilizing mutations may explain rare cases of patient thrombocytopenia.

PLAIN LANGUAGE SUMMARY

Thrombopoietin is a protein and a hormone that is predominantly produced in the liver. Thrombopoietin helps the body to produce different types of blood cells, especially platelets. Platelets are important for the formation of blood clots in the setting of bleeding. Patients with low levels of thrombopoietin can have spontaneous and excessive bleeding, which can be severe and even life-threatening. Therefore, it is important to understand how the body controls thrombopoietin levels. We discovered a new laboratory mouse that has a very small change in the thrombopoietin gene, but this results in a very big decrease in how much hormone is generated by the liver. These mice also have low platelet levels like many human patients. We hope that this new mouse model can be used to understand how thrombopoietin is regulated in both mice and in humans. Ultimately, we hope that this type of research benefits patients with low platelet counts and other blood disorders.

ARTICLE HISTORY
Received 25 March 2024
Revised 1 December 2025
Accepted 19 November 2025

KEYWORDS
Hematopoietic stem cells; mouse model; platelets; thrombocytopenia; thrombopoietin; transcriptional regulation

Introduction

The hormone thrombopoietin (TPO) is the principal regulator of platelet (PLT) production,[1,2] and plays an important role in maintaining hematopoietic stem and progenitor cell (HSPC) number and

CONTACT Nan Sophia Han nan.sophia.han@ki.se Department of Women's and Children's Health, Karolinska Institutet, Tomtebodavägen 18A, Stockholm 17177, Sweden; David B. Sykes dbsykes@mgh.harvard.edu Massachusetts General Hospital Cancer Center, 55 Fruit Street, Boston, MA 02114, USA.

Supplemental data for this article can be accessed online at https://doi.org/10.1080/09537104.2025.2602721

function during development and adulthood.[3,4] TPO is primarily synthesized in hepatocytes and is rapidly secreted into the blood, where it binds its receptor Mpl (myeloproliferative leukemia protein) on target cells (e.g. platelets). Smaller amounts of TPO are produced in other organs, notably the bone marrow.[5] Following binding to the Mpl receptor, TPO is internalized and removed from circulation.[1,6] The loss of adequate TPO signaling results in thrombocytopenia, which is common in the clinical setting of chronic liver failure where progressive damage to hepatocytes results in low TPO production and ultimately in low platelet counts.[7] Less common causes of decreased TPO include the binding and clearance of circulating TPO by autologous antibodies,[8] and defective Mpl-signaling in congenital amegakaryocytic thrombocytopenia.[9] Absence of compensatory TPO elevation is considered a key pathophysiological mechanism in immune thrombocytopenic purpura (ITP).[10]

Several animal models have been used to study thrombopoietin deficiency. The earliest and most widely used mouse strains are the global germline knockouts of the *Thpo* and *Mpl* genes, in which neomycin resistance cassettes are used to disrupt the genomic loci.[11–13] Later work generated mice with conditional TPO knockout specific to hepatocytes or to bone marrow,[14] gene silencing of hepatic TPO transcripts using antisense oligonucleotides,[15–17] and a zebrafish model facilitating the high-throughput screening of patient TPO variants and drug candidates.[18] While these models have advanced insights into TPO biology, they share a key limitation: disruption of the genomic locus (or the RNA product in the case of antisense oligonucleotides) precludes investigation of transcription and transcriptional regulation. Growing evidence suggests that, contrary to previous belief, TPO may be regulated at the RNA level in health and disease.[19–21] Furthermore, germline TPO knockouts display total loss of circulating protein (or a ~50% reduction in the heterozygote mice), where neither homozygotes nor heterozygotes are entirely reflective of the TPO and platelet levels seen in human conditions such as clinical liver disease with intermediate TPO-deficient thrombocytopenia.[22,23]

Here, we describe a new mouse strain bearing a novel and spontaneously arising single base pair mutation in exon 5 of *Thpo*. This mutation was unexpectedly discovered in a colony of *Pcyox1lem1 (IMPC)J* mice, a knockout (KO) model of the gene prenylcysteine oxidase 1-like (PCYOX1L). This single base pair change results in a single amino acid change, with a predicted major alteration in protein conformation, ultimately leading to a >95% decrease in circulating TPO and impaired TPO-Mpl binding. The mutation (leucine to histidine at position 121) is located in the N-terminal erythropoietin-like (EPO-like) domain of the protein, a highly conserved region responsible for the binding of TPO to its cognate receptor Mpl.[1,24] The hematological phenotype of this new strain mimics that of other global TPO knockouts, but the genomic locus is intact, and TPO transcriptional regulation is preserved. We present our characterization of the TPO point mutation and the hematological phenotype of the mouse and discuss its possible applications as a new model of thrombocytopenia.

Methods

Mouse models

All experiments involving mice were performed in accordance with the Institutional Animal Care and Use Committee guidelines at the Massachusetts General Hospital. Wild-type controls were C57BL/6 mice purchased from Charles River Laboratories (Wilmington, USA) unless otherwise stated.

The *Pcyox1lem1(IMPC)J* mouse was made at Jackson laboratories (Bar Harbor, USA) on a C57BL/6 background. CRISPR/Cas9 was used to target exon 3 of the *PCYOX1L* gene, resulting in a deletion of 469 base pairs and in an amino acid change at residue 99 with early termination of the protein at residue 112. Rederivation was done by the Mutant Mouse Resource and Research Centers (MMRRC) at the University of California Davis.

The *C57BL/6-CD45.1*^{STEM} congenic mouse strain used in the competitive transplant assays was previously developed at our lab.[25] The *Thpo*$^{-/-}$ and *Thpo*$^{+/-}$ mice were a kind gift from Dr Elisabeth Battinelli.

As of May 2024, the *C57Bl/6(IMPC)J-TPO*^{L121H} mouse strain has been cryopreserved at Charles River Laboratories (https://www.criver.com/), line ID: 95 073.

Mouse genotyping

PCYOX1L and TPO genotyping was performed by Transnetyx (Memphis, Tennessee).

Euthanizing mice and collecting tissues

Mice were anesthetized using isoflurane. Peripheral blood sampling was conducted retro-orbitally or by cardiac puncture, into EDTA-coated tubes. For serum samples, blood was collected into Eppendorf tubes, allowed to clot at room temperature for 2 h, and centrifuged at 20 000 ×g for 20 min. Mice were euthanized by CO_2 asphyxiation followed by cervical dislocation, and organs and bones were collected. Bone marrow was extracted from femur and tibia by cutting the bone at the geniculate epiphysis and centrifuging at maximum speed for 30 s into collection buffer (PBS with 2% FBS and 1 mM EDTA). All subsequent centrifugations of cells and tissues were performed at 500 ×g for 5 min. Spleen and liver were macerated on ice through a 70 µm filter into collection buffer and centrifuged. Complete blood counts (CBCs) were performed on the Heska Element HT5 analyzer.

Red blood cell (RBC) lysis of blood, bone marrow, and spleen was performed by 5 min incubation with ACK lysis buffer (cat# 118–156–721, Quality biological). Blood, bone marrow, and spleen cells were counted with 1:1000 acridine orange using the Cellometer Vision (Nexcelom Bioscience). Liver samples were weighed. For RNA extraction, an appropriate cell number or tissue volume was immediately lysed in buffer RLT with 1% beta-mercaptoethanol and homogenized by QIAshredder (cat# 79 656, Qiagen) before proceeding to RNA extraction or storage at −80°C. Protein lysates were prepared at 2–10 × 10^6 cells/mL or 30–50 mg tissue/mL. For RIPA-based lysates, sample was resuspended in 1X RIPA buffer (Cell Signaling Technologies) with 1% 100X protease/phosphatase inhibitor cocktail (cat# 5872, Cell signaling technologies), homogenized by QIAshredder, incubated on ice for 30 min with vortexing every 5 min, and centrifuged to collect supernatant for storage at −80°C. For preparation of LDS-based lysates, sample was resuspended in 1X NuPAGE LDS sample buffer (cat# NP0008, Novex) with 1% beta-mercaptoethanol, homogenized by QIAshredder, boiled for 1 min at 95°C, and immediately stored at −80°C.

Flow cytometry

For HSPC flow cytometry, the bone marrow cells were incubated for 30 min at 4°C with the following BioLegend antibodies in collection buffer: c-Kit-PE, CD34-FITC, Sca-1- BV421, CD16/32- BV605, CD48- APC-Cy7, CD150-APC, CD45.1- BV510, CD45.2- BV785, and anti-Lin cocktail. The cells were then washed and incubated for 30 min at 4°C with streptavidin-BV650, and 7AAD (BD Pharmingen) was used for viability staining. Flow cytometry was performed on a BD FACSCelesta instrument (serial# R 660 34400581, model number 660344). The data was analyzed using FlowJo software (v10.10). For CD45.1/2 chimerism checks, the cells were incubated with BioLegend CD45.1-FITC and CD45.2-APC for 30 min at 4°C.

Adult competitive transplant assay

Unless otherwise stated, adult recipients and donors were 19–22 weeks old, and all donors were age- and sex-matched. On the morning of transplant, CD45.1/2 heterozygous recipient mice were lethally irradiated with two doses of 475 cGy separated by 4–6 h. Three CD45.1 *STEM* and three CD45.2 *C57Bl/6(IMPC) J-TPO*^{L121H} donor mice were euthanized. CBCs were used to assess donor platelet levels (Heska Element HT5). Bone marrow was extracted from femurs and tibias as described above. After ACK lysis to remove red blood cells, flow cytometry was used to confirm the individual HSC phenotype. The CD45.1 and CD45.2 cells were then pooled, counted with acridine orange, and combined at a 1:1 ratio to 10 million cells/mL. Each irradiated recipient was injected retro-orbitally with 200 µL cell mix, or 2 million cells, within 3 h of irradiation. The remaining cell mix was analyzed by flow cytometry to confirm the transplanted ratio of CD45.1 and CD45.2 cells. During the first week post-transplant, the mice were observed carefully and

received a fresh hydrogel every day. Every 4 weeks, the mice were anesthetized using isoflurane gas and approximately 100 μL peripheral blood collected retro-orbitally for CBCs and flow cytometry to track CD45.1/CD45.2 chimerism. The mice were euthanized 20 weeks after transplantation, and blood and bone marrow were collected for CD45.1/CD45.2 and HSC flow cytometry.

Homing assay

Methodology for homing largely follows that described above for adult competitive bone marrow transplant. Based on previously published protocols,[26–28] 20 million total bone marrow cells were injected retro-orbitally into each recipient. The recipients were euthanized 24 h post-transplant, and blood, bone marrow, and spleen were collected for CD45.1/CD45.2 and HSC flow cytometry.

Timed pregnancies and harvest of fetal livers

Breeding pairs were created with 12-week-old heterozygous CD45.2 *C57Bl/6(IMPC)J-TPO*^{L121H}mice. Females were housed together for 12 days, and males 5 days. Bedding from the male cage was introduced to the female cage 2 days in advance. On the day of breeding, the females were separated, and one male was added to each female cage. The next day the males were removed from the cages, and the females checked for vaginal plugs. The females were weighed every other day to follow the pregnancy. After 15 days, the pregnant mice were euthanized, and embryonic day 15.5 fetuses were collected. The livers were dissected, macerated through a 40 μm filter using a plunger, incubated with ACK lysis buffer, transferred through a 70 μm filter, washed in collection buffer (PBS with 2% FBS and 1 mM EDTA), and frozen at −80°C in 80% FBS and 20% DMSO. Upper limbs were collected for genotyping.

Bone marrow hematoxylin-eosin staining

Femurs were dissected as described above and embedded in 10% buffered formalin phosphate (SF100-4, Fisher Chemical). Decalcification, longitudinal sectioning, and hematoxylin-eosin staining were performed at the Massachusetts General Hospital Histopathology Research core facility. Images were captured using the Infinity2 camera and Lumenera software v 6.5.5.

Western blot

The protein concentration of RIPA-based lysates was quantified by the QuantiPro BCA Assay kit (cat# QPBCA, Sigma-Aldrich) according to manufacturer protocol. After normalization of protein amount and addition of NuPAGE LDS sample buffer with 1% beta-mercaptoethanol, samples were boiled for 3 min at 95°C, loaded in NuPAGE 4–12% Bis-Tris gel (NP0323, Invitrogen) alongside ladder and run in MES-SDS Running buffer (cat# 21 420 036, Bioworld) at 100 V until the dye front reached the bottom of the gel. Wet transfer was performed onto methanol-activated Immobilon transfer membrane (cat# IPFL07810, Millipore) in 1X transfer buffer (BP-190, Boston Bioproducts) for 100 min at 100 V. After transfer, the membrane was air-dried, activated in methanol, washed with molecular grade water, soaked in PBS, and blocked on a rocker with blocking buffer (Intercept blocking buffer TBS [cat# 927– 60 001, LICOR] or 5% milk) for 1 h at room temperature. Primary antibody mix was prepared in blocking buffer and used to stain the membrane overnight at 4°C on rocker. The next day, secondary antibody mix was prepared – for LICOR system IRDye 680 anti-mouse (cat# 926– 68 020, LICOR) or IRDye 800 anti-rabbit (cat# 926– 32 211, LICOR) in PBS blocking buffer (cat# 927– 70 001, LICOR) with 0.2% Tween-20 and 0.01% SDS. For iBright system 1:3000 HRP-conjugated anti-rabbit secondary (cat# 1 706 515, Bio-Rad) in 5% milk. The membrane was washed for 5 min × 3 in 1X TBS with 0.1% Tween-20 and stained in the secondary antibody mix for 1 h at room temp, on rocker and protected from light. After a final four washes and rinse in PBS, the membrane was air-dried and imaged using the LI-COR Odyssey CLx-2000 machine with the Image Studio software, or using the iBright FL1000 (ThermoFisher) with chemiluminescent detection and the Invitrogen iBright Analysis Software.

Primary antibodies used were mouse monoclonal anti-beta-actin (cat# 8H10D10, Cell signaling technologies) at 1:1000, rabbit polyclonal anti-PCYOX1L at 1:1000 (cat# HPA037463, Sigma-Aldrich), mouse monoclonal anti-GAPDH at 1:10 000 (cat# ab8245, Abcam), rabbit anti-human protein C-tag (cat# GTX18591, Genetex) at 1:1000, and rabbit polyclonal anti-TPO (cat# PA5-80125, Invitrogen) at 1:1000.

Thrombopoietin ELISA

Serum samples were analyzed using the R&D systems Mouse Thrombopoietin Quantikine ELISA kit (cat# MTP00) according to manufacturer protocol. Absorption was read at 450 nm using the Synergy HTX multi-mode reader (BioTek) and the Gen5 software (v.2.07).

RNA extraction

RNA was extracted using the Qiagen RNeasy plus mini kit (cat# 74 134), Qiagen Allprep DNA/RNA mini kit (cat# 80 204), or Qiagen RNEasy micro kit (cat# 74 004). Manufacturer protocol was followed. The optional incubation step with RNase-free DNase (1023460, Qiagen) was included when using the RNeasy kits. RNA content was measured using a Nanodrop spectrophotometer.

Genomic DNA extraction

Genomic DNA was extracted using the Qiagen Allprep DNA/RNA mini kit (cat# 80 204). Manufacturer protocol was followed. DNA concentration was measured by Qubit dsDNA HS kit (cat# Q32851, Invitrogen)

cDNA synthesis

cDNA synthesis was performed using the High-capacity cDNA reverse transcription kit without RNase inhibitor (4368814, Applied biosystems). Manufacturer protocol was followed. 0.5 or 1 µg of RNA was used per 20 µL cDNA synthesis reaction. The thermal cycler (Bio-Rad T100 Thermal cycler, serial# 621BR65037) was programmed to annealing for 10 min at 25°C, elongation for 120 min at 37°C, and denaturing for 5 min at 85°C.

Polymerase chain reaction (PCR)

PCR was carried out using the New England Biolabs Q5 Hot Start High-Fidelity DNA polymerase (cat# M0493), with Q5 reaction buffer (cat# B90275, New England biolabs). For each 25 µL reaction, 50 ng cDNA or genomic DNA was mixed in with 0.5 µM each of primers and 0.2 mM dNTP (cat# BJ6301A, TakaRA). The thermal cycler (Bio-Rad T100 Thermal cycler, serial# 621BR65037) was programmed to denaturation for 10 sec at 98°C, annealing for 30 sec, extension for 30 sec/kb at 72°C, and final extension for 2 min at 72°C. Optimal annealing temperature was calculated by the online NEB Tm Calculator, and annealing temperature gradients were performed for further optimization when necessary.

Real-time PCR (RT-PCR)

iTaq Universal SYBR Green Supermix (cat# 1 725 121, Bio-Rad) was used for RT-PCR. Per 20 µL reaction, 10 µL of SYBR Supermix was combined with primer to a final 0.5 µM concentration each and 20 ng of cDNA or genomic DNA. The thermal cycler (Bio-Rad CFX96 Real-time System, serial# CT041759) was programmed according to manufacturer instructions. Beta-actin was used as housekeeping gene.

Table 1. Primer sequences used for long-range PCR, PCR, and qPCR of *Thpo*.

Thpo- Long-range qPCR primers, used to amplify genomic DNA for sequencing		
Primer pair	Forward primer	Reverse primer
1 (2)	GGAAGAGAGGAGCCAGCAAAGAGGTATTT	TGGTCCCTGATTTTTATTGGCTTTTGGG
2 (3)	GCTGGAGGATGAGGACTTGTCTTTGAAAAT	TTTACAATCTCCAGTGCTGTGTATCCCTTC
Thpo- PCR primers, used to amplify cDNA for sequencing		
1 (NSH)	CTGTGACCCCAGACTCCTAAAT	CGCTATGTTTCCTGAGACAAATTC
2 (DBS)	TGCTGTGGACTTTAGCCTGG	CTTTGTTGAAAGCTCCGGGC
Thpo- qPCR primers, used to quantify TPO mRNA levels		
1 (1)	GGCCATGCTTCTTGCAGTG	AGTCGGCTGTGAAGGAGGT
2 (4)	CTCATGGGCTCTTTGCTGGA	AAGGGTGTGTGTCCATCAGG

Long-range PCR

Long-range PCR was performed using the New England biolabs LongAmp HotStart Taq DNA polymerase (cat# M05345), with LongAmp 5X Taq buffer (cat# B03235, New England biolabs). For each 25 µL reaction, 50 ng genomic DNA was mixed in 0.3 mM dNTPs, 0.4 µM of each primer, and 2.5 units DNA polymerase. The thermal cycler (Bio-Rad T100 Thermal cycler, serial# 621BR65037) was programmed to initial denaturation for 30 s at 94°C, 35 cycles of denaturation for 30 s at 94°C, annealing for 30 s, extension for 50 s/kb at 65°C, and final extension for 10 min at 65°C. Optimal annealing temperature was calculated by the online NEB Tm Calculator, and annealing temperature gradients were performed for further optimization when necessary.

Primers for PCR, RT-PCR, and long-range PCR (Table 1) were designed using the Primer design and Quicktest primer functions in MacVector and ordered through the ThermoFisher Custom DNA Oligos Synthesis Services.

Agarose gel electrophoresis and gel extraction

0.8% or 2.0% w/v agarose gels were prepared with agarose powder (cat# BP1356-500, Fisher bioreagents), 1X TAE buffer (cat# BM-250, Boston bioproducts), and 1:12000 ethidium bromide (ThermoFisher) or SYBR safe DNA gel stain (cat# S33102, Invitrogen). 25 µL of PCR or long-range PCR product was loaded with blue/orange loading dye (cat# G190A, Promega) alongside 1 kb ladder (cat# N32325, New England biolabs) or 100 bp DNA ladder (cat# N32315, New England biolabs). The gel was run at 100 V until the dye front reached the bottom. Ethidium bromide gels were imaged by Proteinsimple (Bio-Techne) using the AlphaImager HP software, and SYBR safe DNA gels were imaged by blue light. Bands were resected using a clean scalpel, and DNA was purified by the Qiaquick gel extraction kit (cat# 28 704, Qiagen) according to manufacturer protocol. DNA content was measured by Qubit dsDNA HS kit.

Sequencing of PCR products

Sanger sequencing of PCR products was performed by the Massachusetts General Hospital Center for Computational and Integrative Biology DNA core facility. Long-range PCR products were sequenced commercially through the Plasmidsaurus linear/amplicon sequencing service.

Statistics

Sample sizes for mouse experiments were determined by prospective sample size estimation and experience from prior similar work. *P*-values were calculated by unpaired student t-test in Graphpad Prism (v.9.5.1), statistical significance was determined as p-value $< .05$. Error bars represent SD in all graphs.

Database searches

GnomAD data was retrieved between June and August 2023.[29] Query of UK biobank exomes was performed by Dr Vijay G. Sankaran.

Protein structure predictions

The sequence of the TPO gene was acquired using Entrez.[30] Prediction of three-dimensional protein structure was performed using the online AlphaFold2 colab server (ColabFold v1.5.5: AlphaFold2 using MMseqs2 https://colab.research.google.com/github/sokrypton/ColabFold/blob/main/AlphaFold2.ipynb#scrollTo=11l8k–10q0C).[31] PDB files were exported and visualized using UCSF Chimera, developed at the University of California San Francisco with support from NIH P41-GM103311.[32]

Single-cell analysis

The murine bone marrow single cell data and cell annotations were downloaded from the Gene Expression Omnibus (GEO) database GSE188902.[33] The Conos approach[34] was used to integrate multiple scRNA-seq datasets with default setting (PCA space with 30 components, angular distance, mNN matching, k = 15, k.self = 5). UMAP embedding was used to visualize PCYOX1 and PCYOX1L expression.

Sequence alignment using MacVector

The sequences of murine and human TPO were downloaded from Entrez and aligned using MacVector software.

TPO plasmid design

Plasmids were designed with the open reading frame of native and L121H-mutant TPO respectively conjugated to DYKDDDDK/FLAG tag. The constructs also contained an eGFP separated by an IRES sequence. The plasmids were designed and synthesized by VectorBuilder.

Cycloheximide chase assay

3×10^5 HEK293T cells (ATCC, cultured in DMEM with 10% FBS) were seeded into each well of a 6-well plate. The next day, the cells were transfected with TPO WT/L121H-FLAG-IRES-eGFP constructs at 3 μg/well using a standard 3:1 ratio of Lipofectamine 3000 (cat# L3000001, ThermoFisher) to plasmid DNA and incubated overnight. On the third day, each well was treated with 100 μg/mL cycloheximide (cat# C4859, Sigma-Aldrich) in pre-warmed DMEM with 10% FBS, according to the determined time course. After 24 h, all wells were simultaneously trypsinized and counted using trypan blue. RIPA-based lysates were prepared and Western blot performed as described above. Membranes were stained with 1:1000 DYKDDDDK tag (FLAG tag) rabbit monoclonal primary antibody (cat# D6W5B, Cell signaling technologies) and imaged using iBright FL1000 with chemiluminescent detection.

Synthesis of recombinant TPO proteins

Recombinant WT and L121H mutant TPO protein were synthesized by Protein Production Sweden (PPS), a national infrastructure funded by the Swedish Research Council, according to their standard workflow.[35] In short, constructs of the biologically active portions of WT and mutant TPO were tagged with a C-terminal human protein C purification tag. CHO cells were chosen for protein expression as they demonstrated superior yield compared to HEK293T cells. The proteins were harvested from cell culture supernatant and purified by affinity chromatography with a protein C-tag antibody matrix. Protein concentrations were determined by absorbance at 280 nm, and analysis of protein purity and identity

were performed by SDS-PAGE electrophoresis and Western Blot. The yield of WT TPO was 195 µg/mL (total 585 µg) and mutant TPO 33 µg/mL (total 56 µg).

HEK-Blue™ TPO bioactivity reporter assay

TPO biactivity was assessed according to manufacturer protocol. In short, HEK-Blue™ TPO reporter cells (InvivoGen, cat# hkb-tpo, cultured in DMEM with 10% FBS) were seeded at 50 000 cells/well in 96-well plates and incubated overnight at 37°C with the desired concentration of recombinant WT and TPO^{L121H} protein. The next day, 20 µL cell supernatant was transferred to a fresh 96-well plate and incubated with QUANTI-Blue solution for 30 min to 3 h. Optical density was measured at 620 nm using a Varioskan LUX microplate reader.

Results

A spontaneous point mutation in TPO is identified in the background of an unrelated mouse strain

This project began when our team was asked to characterize the hematopoietic compartment of the *Pcyox1lem1(IMPC)J* mouse strain. Originally generated by Jackson Laboratories, this strain was established by the CRISPR-Cas9 mediated knockout of *PCYOX1L* on a C57Bl/6 background. Unexpectedly, these mice were noted to have an affected hematological phenotype with pronounced thrombocytopenia but otherwise normal blood counts (Figure 1(A)). Upon examination of the bone marrow, there was also a near-complete loss of long-term hematopoietic stem cells (HSCs) (Figure 1(B)).

These findings were intriguing because little is known about the enzyme PCYOX1L. PCYOX1L has significant sequence homology with family member prenylcysteine oxidase 1 (PCYOX1) and is predicted to be involved in the enzymatic breakdown of prenylated proteins.[36] The loss of PCYOX1L has been shown to impact neutrophil bactericidal activities.[37] Consistent with a potential role in hematopoiesis, PCYOX1L is differentially expressed in developing bone marrow hematopoietic cells (Figure 1(C)). We hypothesized that the loss of PCYOX1L may lead to a toxic accumulation of prenylated proteins within hematopoietic progenitors and therefore might account for the observed HSC and PLT phenotype.

As we began characterizing the mice, we crossed the PCYOX1L KO mouse onto the background of our $CD45.1^{STEM}$ mouse strain[25] , to establish a congenic strain for easy *in vivo* tracking of hematopoietic cells in competitive bone marrow transplant experiments. Unexpectedly, crossing these mice revealed a discordance between PCYOX1L genotype and hematological phenotype. Specifically, some mice lacking PCYOX1L had a wildtype (WT) hematological phenotype, and other mice with WT PCYOX1L expression displayed the affected hematological phenotype with low HSC and PLTs (Figure 1(D)).

These findings supported a new hypothesis that the loss of PCYOX1L was unrelated to the hematopoietic phenotype. Indeed, in discussion with the mouse vendor, we obtained complete blood count data from the original PCYOX1L KO strain that had been collected prior to sperm cryopreservation. In these original PCYOX1L KO mice, the PLT levels were normal (Figure 1(E)). This suggested that the aberrant PLT and HSC phenotype within the strain most likely developed during or after the rederivation process.

A single base pair **Thpo** *mutation identified in mice with low platelet counts*

The discordance between PCYOX1L expression and the PLT/HSC phenotype prompted us to consider alternative hypotheses. Bone marrow sections from the affected mice displayed a near complete absence of megakaryocytes, suggesting that the low platelet counts were due to a production defect rather than a destructive process (Figure 2(A)). Given the critical role of TPO in megakaryocyte development and platelet production, we decided to quantify serum TPO, revealing that TPO levels were ~95% reduced in the affected mice (Figure 2(B)). Notably, the low serum TPO levels of these mice were distinct from the undetectable TPO levels within conventional germline *Thpo* knockout mice.[12] We concluded that low circulating TPO levels were the likely explanation for the reduced bone marrow HSCs and low platelet counts.

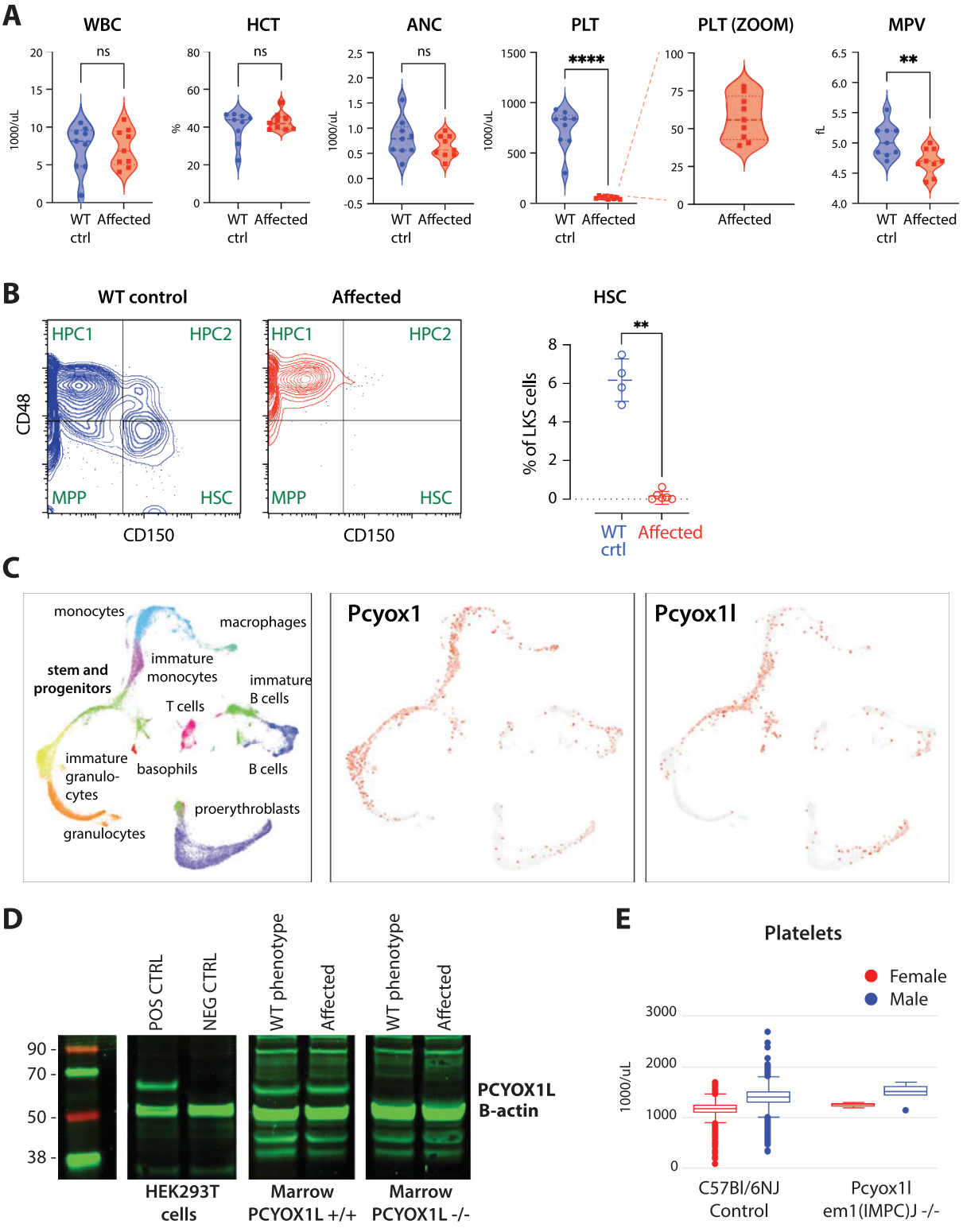

Figure 1. Hematopoietic characterization of the putative PCYOX1L knockout mouse. (A) Isolated thrombocytopenia. Affected mice had a ~ 15-fold reduction of platelet counts (PLT), with slightly reduced mean platelet volume (MPV). Peripheral blood counts were otherwise unaffected. ($n = 9$ for each group). (B) Loss of hematopoietic stem cells. Flow cytometric analysis of bone marrow showed a near-complete loss of phenotypic long-term hematopoietic stem cells (Lin^{neg}, c-Kit^{pos}, $Sca1^{pos}$, $CD150^{pos}$, $CD48^{neg}$) in the affected mice. (C) Gene expression of PCYOX1 and PCYOX1L in hematopoietic cells. UMAP visualization of single-cell transcriptomic data of murine bone marrow showing PCYOX1L is expressed in hematopoietic stem and progenitor cells, and that expression decreases as cells mature. (D) Genotype-phenotype discordance. PCYOX1L expression did not correlate with the hematological phenotype in some mice. Protein expression was verified by Western blot. (E) The original *Pcyox1lem1(IMPC)J* strain was hematologically normal. Data from the Jackson Laboratories Early Phenotyping Study, collected prior to sperm cryopreservation, shows that the original *Pcyox1lem1(IMPC)J* strain ($n = 6$ for each sex) had platelet counts comparable to wild-type controls ($n =$ ~2000 for each sex).

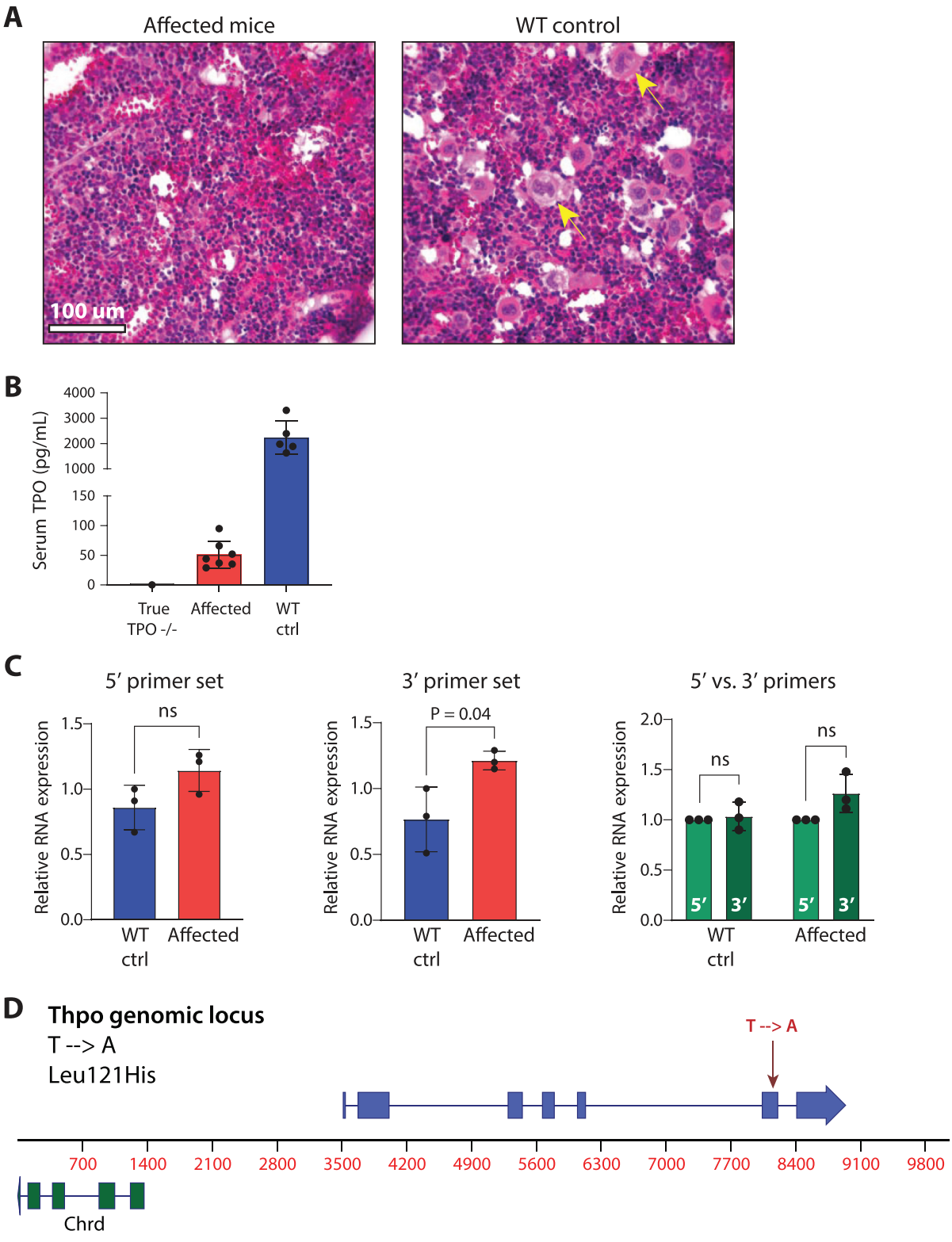

Figure 2. Identifying a novel TPO^{L121H} mutation. (A) Loss of megakaryocytes. Hematoxylin-eosin staining of femur sections showed that affected mice have a loss of megakaryocytes in the bone marrow (yellow arrows), verified by manual counting of multiple images (data not shown). 40X magnification. (B) Low serum TPO concentration. The affected mice had a ~ 95% reduction of circulating serum TPO as measured by ELISA ($n = 7$), though not to the undetectable levels of the conventional TPO knockout mouse ($n = 1$). (C) Intact TPO transcription. Total hepatic TPO mRNA was quantified by RT-PCR. Two primer sets that targeted the 5′ and 3′ ends of the TPO mRNA transcript were compared to detect any potential truncation of the transcripts. (D) L121H mutation. Genomic DNA from bone marrow and liver lysates as well as cDNA from liver was sequenced. A single T to A mutation was identified at position 362 of the TPO open reading frame, corresponding to a leucine to histidine mutation at position 121 of the mRNA.

Furthermore, we discovered that unlike in established TPO-deficiency models,[12] hepatic TPO mRNA expression was not only equivalent but slightly elevated in the affected mice compared to WT controls, arguing against a promoter mutation or other defect in TPO transcription (Figure 2(C)). Finally, sequencing of the ~10 000 base pair genomic locus of *Thpo* in the affected mice revealed a single T to A nucleotide mutation at position 362 in the open reading frame (Figure 2(D)). This T362A mutation was further confirmed at the mRNA level by Sanger sequencing of amplified cDNA prepared from total liver RNA.

The murine *Thpo* and *PCYOX1L* genes are located on separate chromosomes (16 and 18, respectively). As the mice had been generated using CRISPR/Cas9 technology, we hypothesized that the mutation might have arisen due to an off-target effect. Re-analysis of the guide design and possible off-target sites did not identify any likely sites within the *Thpo* locus. Ultimately, we surmised that during the process of rederivation from frozen sperm, our *Pcyox1lem1(IMPC)J* mouse unexpectedly acquired a spontaneous single base pair mutation in the *Thpo* gene, leading to the dramatic reduction of circulating TPO.

TPO protein structure is dramatically altered by the single leucine to histidine amino acid alteration, leading to reduced TPO-Mpl binding activity

We next queried how a single amino acid change could cause a ~ 95% loss of circulating TPO. The T362A base pair mutation results in a non-synonymous, non-conservative amino acid change from the uncharged leucine to the positively charged histidine. The mutation is located on residue 121 in the EPO-like domain of the TPO protein, a conserved and highly structured region composed of four alpha-helices.[1] To predict the effect of this L121H mutation on protein conformation, we utilized AlphaFold2 (ColabFold v1.5.5)[31] to generate three-dimensional protein structure predictions of native and L121H-mutated TPO. These predictions suggested a striking conformation change in the mutant protein, where the N-terminal alpha-helix was displaced from its original position (Figure 3(A)).

We hypothesized that the L121H mutation and resulting change in protein structure could trigger the loss of TPO through various post-transcriptional mechanisms, including rapid degradation of the destabilized protein upon entering blood circulation. However, we found no difference in WT and mutant protein half-life by cycloheximide chase assay (Figure 3(B)). We then speculated that the mutation might cause a secretion defect, trapping TPO intracellularly. When we assessed the 293T cells used to generate recombinant WT and L121H TPO by Western blot, it appeared that intracellular production of the mutant protein was dramatically reduced compared to the WT protein (Figure 3(C)). This phenotype may have been due to differences in transient transfection efficiency as a simple explanation, but may also suggest that the mutation causes TPO loss through impaired translation or rapid degradation following translation.

Given the striking alteration in protein structure, we proceeded to investigate whether the TPO L121H mutation impaired the binding of TPO to its cognate receptor Mpl in addition to decreasing circulating TPO levels. Recombinant WT and TPO^{L121H} proteins were synthesized through the Protein Production Sweden national infrastructure. The functional activity of the WT and mutant proteins was quantified using a TPO reporter cell line (HEK-Blue™ TPO reporter cells, InvivoGen). We found that the L121H mutation impaired the ability of TPO to bind and activate Mpl (Figure 3(D)). While activity was observed at very high protein concentrations (>160 ng/mL), the mutant TPO exhibited a 16-fold lower potency as compared to the WT protein (Figure 3(E)).

Hematological characterization of the C57Bl/6(IMPC)J-TPO^{L121H} mice

Consistent with the known function of TPO, CBCs showed an isolated reduction in platelet counts with normal numbers of red and white blood cells in adult mice (Figure 1(A)), and bone marrow histology displayed loss of megakaryocytes but otherwise normal marrow morphology (Figure 2(A)).[4,38] Tail bleeding times were not performed as ~90% reduced platelet count to ≥25 000/μL (Figure 1(A)) was not expected to affect hemostasis in mice.[39] Indeed, the mice did not exhibit spontaneous bruising or bleeding, nor did we appreciate problems in other organ systems or decreased offspring viability. Platelet function was not tested

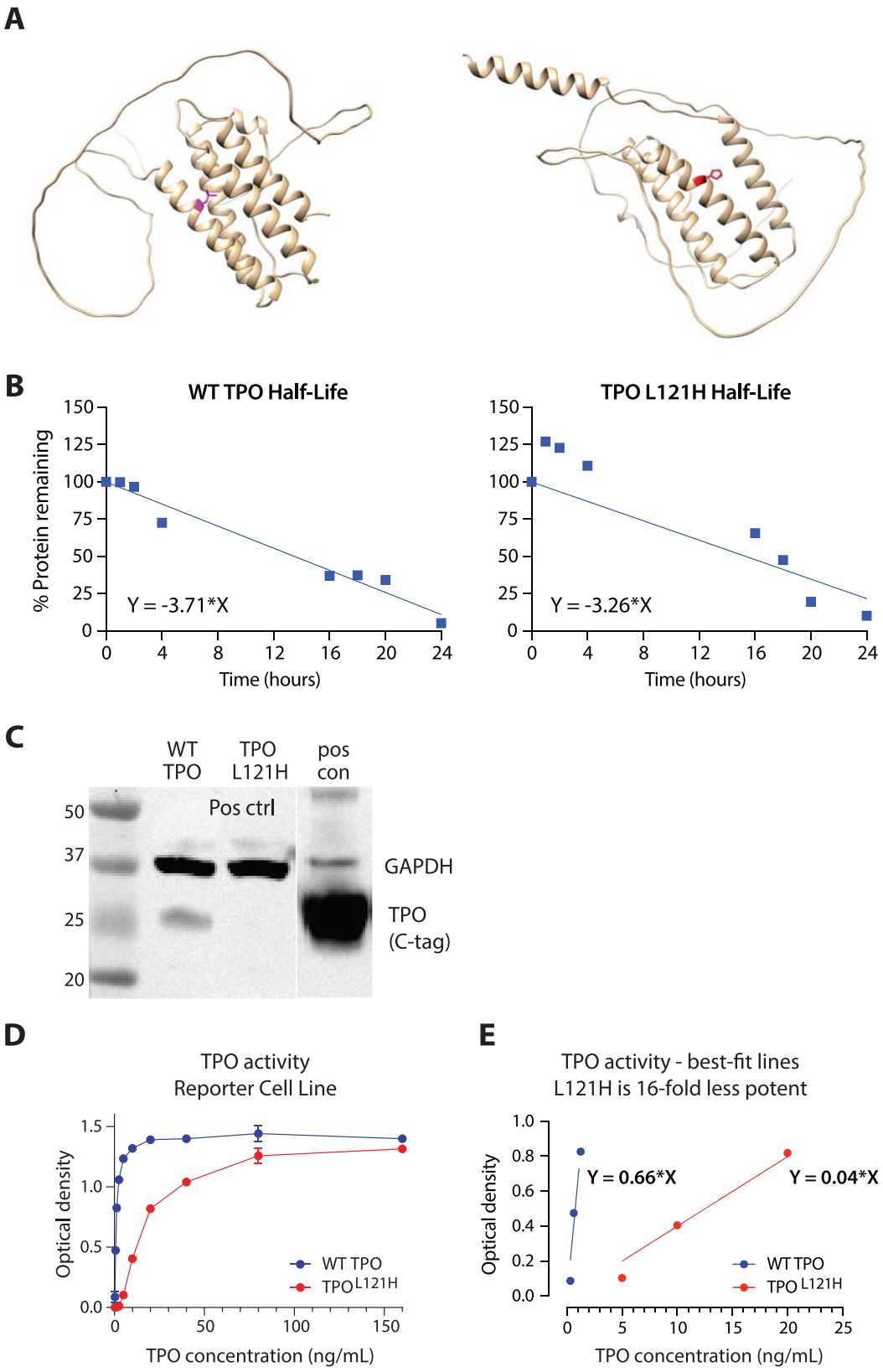

Figure 3. The L121H mutation disrupts TPO structure and function. (A) Protein structure prediction. The L121H mutation alters TPO protein structure by displacing one of the alpha-helices comprising the core of the TPO protein. Leucine in pink, histidine in red. Generated using Alphafold2 and visualized with USCF Chimera. (B) Protein half-life. The half-lives of WT and L121H mutant TPO were not significantly different. HEK293T cells were transiently transfected with a TPO-GFP-FLAG or

but has been previously shown to be normal in *Thpo*$^{-/-}$ and *Mpl*$^{-/-}$ mice.[38,40] Similar to the conventional *Thpo*$^{-/-}$ mice, mean platelet volume (MPV) was slightly decreased (Figure 1(A)).[12]

Bone marrow HSPCs were assessed by flow cytometry (Figure 4(A)). As previously described, adult mice exhibited a near-complete loss of long-term HSCs (Lin^{neg} Kit^{pos} Sca^{pos} [LSK], CD48^{neg}, CD150^{pos}) (Figure 4(B)).[41] The total number of LSK cells were only marginally reduced. The myeloid cell constitution was similar between affected mice and WT adults. The dramatic loss of the LT-HSCs in adult mice (Figure 4(B)) contrasted to the hematopoietic makeup of embryonic day 15.5 fetal liver, where the L121H mice were indistinguishable from WT littermates (Figure 4(C)). This is consistent with previous reports, and it has been suggested that the HSC transition to TPO dependency occurs at a later point of embryonic development.[3,42]

Given the striking loss of phenotypic HSCs, we next assessed *in vivo* HSC function by competitive bone marrow transplant, competing equivalent numbers of total bone marrow cells against the wild-type congenic CD45.1^{STEM} mice.[25] Similarly to conventional *Thpo*$^{-/-}$ mice, cells from the adult L121H bone marrow were markedly inferior in terms of long-term reconstitution capacity (Figure 5(A)).[3,41] The early and pronounced competitive disadvantage of the adult bone marrow led us to investigate if the affected mice had defective homing, the process by which transplanted cells find their way to the hematopoietic organs immediately after transplantation.[28] Unexpectedly, a 24-hour homing assay showed a distinct homing advantage of affected cells to both bone marrow and spleen, most prominently in the mature Lin+ and immature LSK compartments (Figure 5(B)).

The L121H mutation is not identified in human whole exome sequencing data

The EPO-like domain of TPO is approximately 85% conserved between humans and mice,[1] and the triple-leucines at residues 120–122 are identical in the two species (Figure 6(A)). We queried whether some clinical TPO-deficient thrombocytopenias could in fact be caused by aberrant TPO protein structure leading to post-transcriptional issues such as defective translation or increased protein breakdown. No such case reports were identified in the literature. A query of ~500,000 UK Biobank exomes and ~250,000 variants in the Genome Aggregation Database (gnomAD)[29] revealed no individuals harboring a mutation at L121. Of the genotypes in the gnomAD database, only four variants represented a single amino acid change from a hydrophobic to a positively charged residue in the EPO-like domain, in analogy with our leucine to histidine mutation.

Discussion

In the nearly three decades since thrombopoietin was first cloned, its molecular structure, crucial role in platelet and hematopoietic biology, and various therapeutic applications have been extensively studied in animal models and thrombocytopenic patients.[43] Here we present a new mouse model of thrombocytopenia, with a > 95% reduction of circulating serum TPO and dramatically impaired TPO-Mpl binding caused by a single base pair mutation in the EPO-like domain of TPO. The importance of the EPO-like domain for TPO-Mpl binding is well known and critical amino acid residues have been identified,[1,2] with at least one report of a point mutation in this region causing a rare case of familial aplastic anemia.[44] Our findings further emphasize the physiological importance of this highly conserved region and suggest its susceptibility to destabilizing mutations. To our knowledge, this report is unique in identifying a TPO structural variant leading to decreased circulating protein levels and resulting low platelet counts through a post-transcriptional mechanism.

---

a TPO^{L121H}-GFP-FLAG plasmid, treated with cycloheximide time-course to stop protein production, analyzed by Western blot (anti-FLAG tag) and quantified by densitometry. (C) Protein production. L121H-producing cells contain less TPO than the WT control. Lysates of the cells used to produce WT and mutant TPO were analyzed by Western blot against human protein C-tag. Commercial recombinant murine TPO (Peprotech, cat# 315-14) was used as the positive control. (D) Protein activity. The L121H mutant TPO is less potent than the WT TPO protein in terms of activating MPL. Recombinant WT TPO and TPO^{L121H} protein were incubated across several concentrations with HEK-Blue^{TM} TPO reporter cells. (E) Loss of potency. Choosing the best-fit linear data, the L121H mutant TPO is 16-fold less potent than WT TPO in this reporter assay.

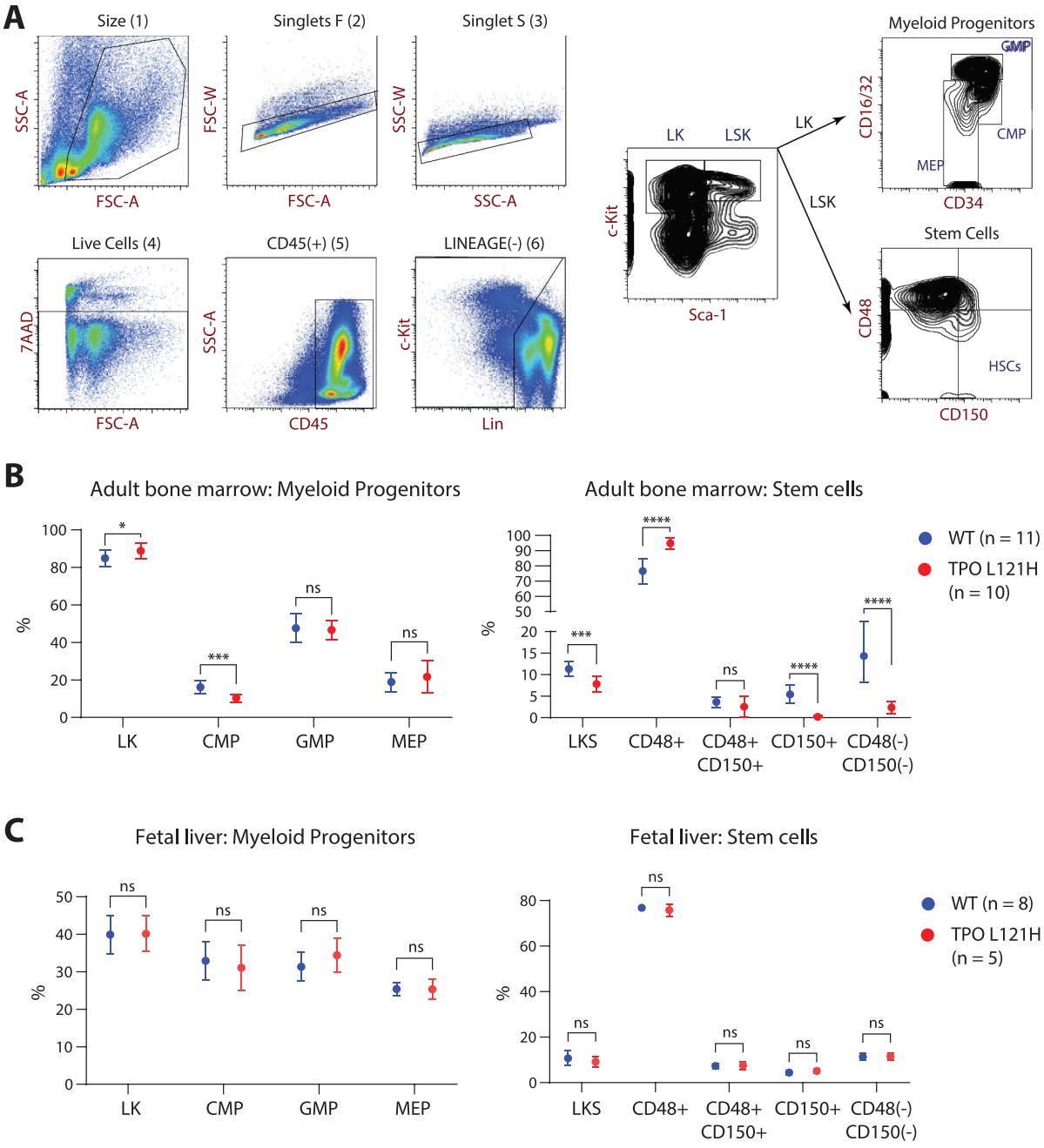

Figure 4. Hematological characterization of the *C57Bl/6(IMPC)J-TPO*^{L121H} mouse. (A) Flow cytometry gating strategy. Depicted in a wild-type C57BL/6 mouse. Staining of CD45, Lin, c-Kit, Sca1, CD16/32, CD34, CD48, and CD150 was used to identify different subpopulations of hematopoietic cells. GMP: Granulocyte-monocyte progenitor. CMP: Common myeloid progenitor. MEP: Megakaryocyte-erythroid progenitor. LK: Lin negative, c-Kit positive. LSK: Lin negative, c-Kit positive, Sca-1 positive. The CD150^{pos}, CD48^{neg} fraction of the LSK cells contain the long-term hematopoietic stem cells. (B) Loss of long-term hematopoietic stem cells. Flow cytometry of adult TPO^{L121H} bone marrow showed near-complete loss of LSK CD48^{neg} CD150^{neg} HSCs. The myeloid progenitors were comparable between the mutant and wild-type animals. (C) Unaffected embryonic hematopoiesis. Flow cytometry of embryonic day 15.5 fetal liver cells did not show any defects in stem or progenitor cell constitution.

We anticipate that our newly-defined mouse model offers a useful tool to dissect the nuances of TPO transcriptional regulation. Unlike conventional knockout models where the genomic locus is significantly disrupted, our model combines TPO protein loss with preserved transcription and transcriptional regulation, as reflected by the intact and even slightly increased levels of hepatic TPO mRNA in the TPO^{L121H} animals. Foundational studies have previously argued against any transcriptional regulation of hepatic

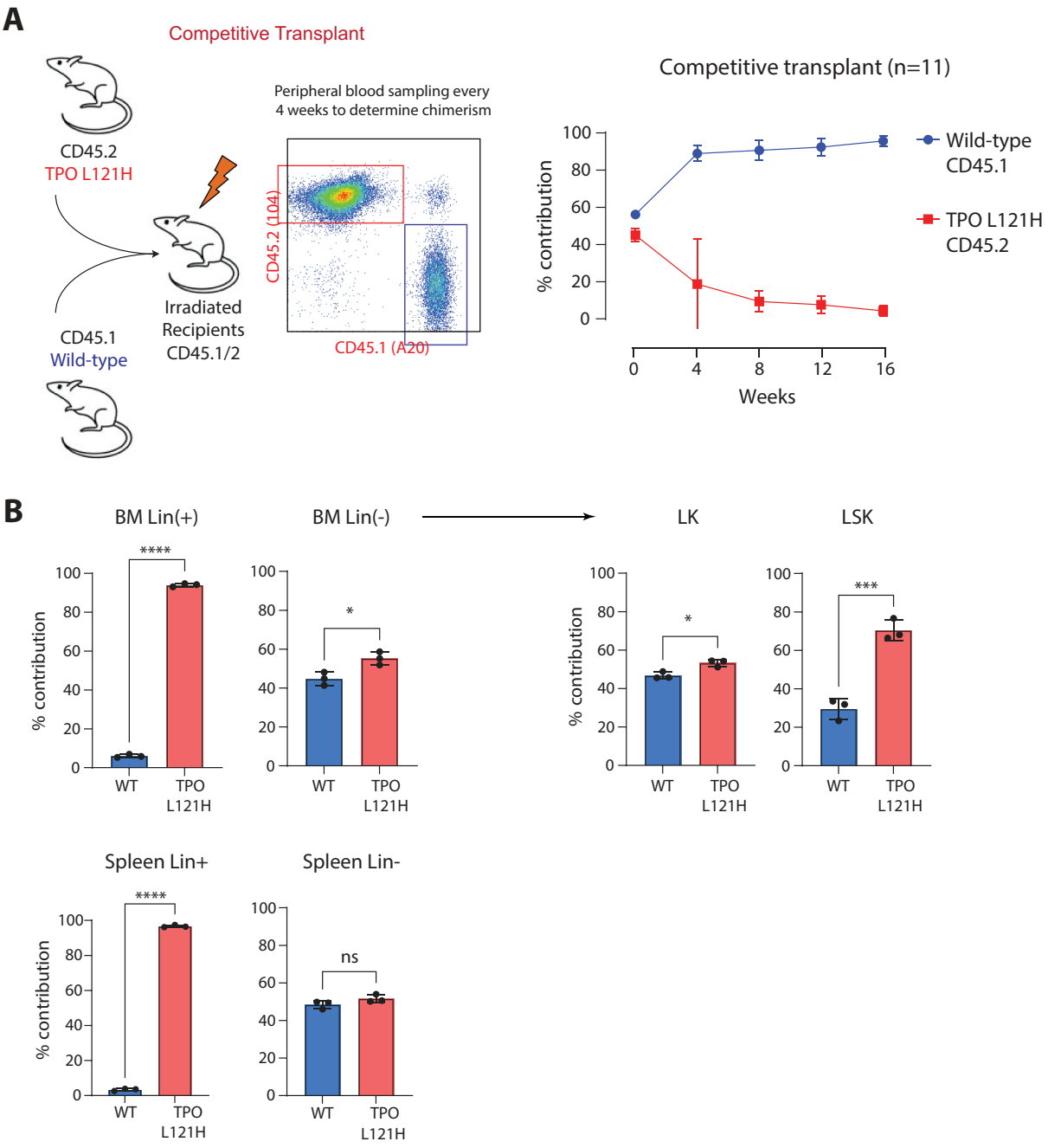

Figure 5. Competitive bone marrow transplant. (A) Defective long-term reconstitution ability. The competitive bone marrow transplant model is schematically depicted to the left. Equal amounts of total bone marrow from CD45.1^{STEM} wild-type donors and CD45.2 TPO^{L121H} donors were transplanted into CD45.1/2 recipients. The peripheral blood CD45 chimerism was followed at 4-week intervals over 20 weeks. Adult TPO^{L121H} bone marrow was inferior in short-term and in long-term reconstitution. (B) Enhanced homing ability. The homing ability of the hematopoietic cells was assessed by competitive bone marrow transplant, with analysis of bone marrow and spleen performed at 24 h post-transplant ($n = 5$). Here, adult TPO^{L121H} bone marrow displays enhanced homing capacity as compared to wild-type cells.

TPO – liver TPO mRNA was found to be completely unaltered in iatrogenic models of severe thrombocytopenia,[45–47] and similarly, hepatic TPO transcripts are not increased in *Mpl*$^{-/-}$ or *Thpo*$^{+/-}$ mice.[12,13] Indeed, there is consensus that the main mechanism of TPO regulation is through direct clearance of circulating protein by *Mpl*-expressing target cells.[3,46,47] However, an expanding body of more recent work has challenged the idea that TPO is exclusively regulated at the protein level in health and disease. In normal physiology, the Ashwell-Morell receptor has been suggested to modulate steady-state hepatic TPO mRNA

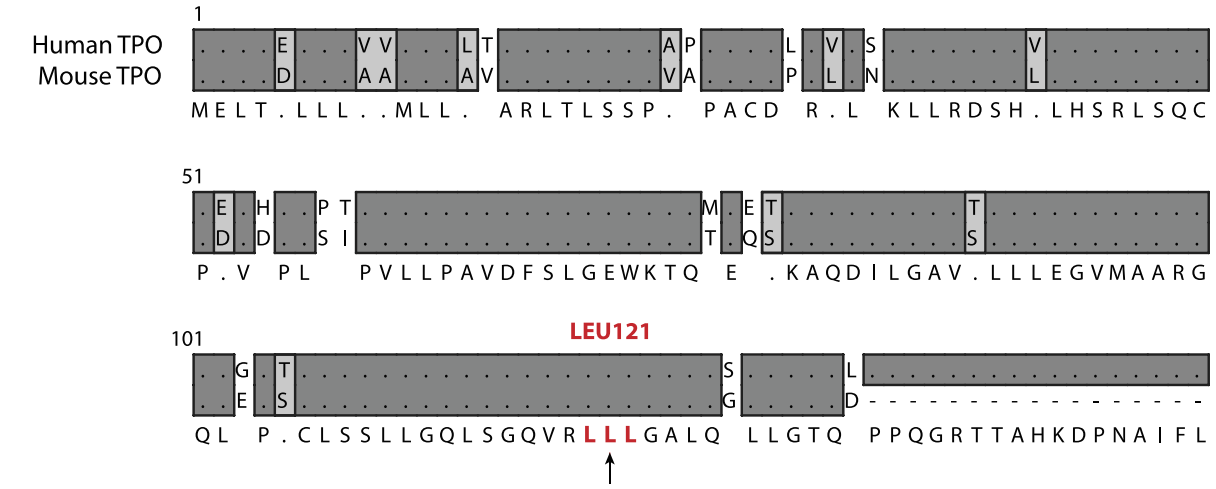

Figure 6. Murine and human TPO sequence alignment. (A) Sequence comparison. The sequences share high similarity, and the affected leucine with its two adjacent residues are completely conserved between the species. Generated using Macvector.

expression.[19] Furthermore, upregulation of hepatic TPO transcription by interleukin-6 (IL-6) has been linked to thrombocytosis in acute inflammatory responses and paraneoplastic phenomena.[21,48,49] Additionally, the small amount of TPO produced in the bone marrow niche, primarily by bone marrow stroma, has been shown to be transcriptionally regulated by platelet demand[5,20,50–52] – the mechanisms of this regulation, and the effect of various endogenous and exogenous stimuli, are not yet fully elucidated. Taken together, there are still unanswered questions about transcriptional regulation of hepatic and bone marrow TPO production, which our mouse may help address.

Given the incomplete loss of TPO in our *C57Bl/6 (IMPC)J-TPO^{L121H}* mouse, we hypothesized that this model could more faithfully recapitulate clinical thrombocytopenias with intermediate TPO loss, compared to the undetectable (*Thpo$^{-/-}$ and Mpl$^{-/-}$*) or halved (*Thpo$^{+/-}$*) TPO levels in conventional KOs. Indeed, some of the most common causes of thrombocytopenia clinically present with moderately reduced platelet counts, such as liver cirrhosis of various etiologies and severity.[7,22,23] It is worth noting that while a wide range of normal mouse serum TPO levels have been reported in the literature (Figure 1(A)),[53,54] our mice have low TPO by most estimates, and most importantly exhibit a marked decrease compared to age-matched littermate controls. The development of a low-TPO system could also contribute to the study of non-hematological platelet-dependent pathologies such as neoplasms,[16] and in theory to reducing hemorrhagic morbidity and mortality in laboratory animals considering the borderline hemostatic competence of conventional *Thpo$^{-/-}$* and *Mpl$^{-/-}$* mice.[4,39] Given the efforts to titrate TPO *in vivo* using invasive and resource-intensive methods such as injections of anti-sense oligonucleotides and baboon-derived anti-TPO autoantibodies,[16,55] our model offers an accessible, consistent, and simplistic alternative.

Whereas the effect of TPO deficiency on HSPCs has been extensively studied,[3,4,14,41,56] the enhanced HSPC homing is a new and unexpected hematological finding. There is *in vitro* and *in vivo* evidence suggesting that TPO could enhance homing by regulating migration- and adhesion-related molecules.[57–59] We hypothesize that TPO-dependent cells in the L121H mice may upregulate cell surface expression of Mpl and thereby outperform WT competitors when transplanted into WT recipients with a normal amount of TPO. This hypothesis remains to be experimentally validated.

Finally, we present the story of this project as equal parts entertaining anecdote and cautionary tale. Our lab received a PCYOX1L knockout mouse with a pronounced hematological phenotype and spent many hours performing experiments, convinced they might yield insights into HSPC biology and protein prenylation. Early genotype-phenotype incongruencies were dismissed as experimental error, and uncooperating Western blot antibodies had us struggling to perform the most basic validation experiments. After more than a year of

efforts, we could finally show that the phenotype was PCYOX1L-independent, which was subsequently confirmed by Jackson Laboratories data that was available to us from day one. With no funds for unbiased whole exome sequencing to identify the source of the problem, we decided to do one last experiment – a "Hail Mary" sequencing of the TPO locus, based off the results of a single ELISA – before officially calling off the project. We did not expect any findings, and instead we discovered a single base pair mutation – a spontaneous T to A, in one of the 2.7 billion base pairs in the mouse genome and one of the ~10,000 base pairs in *Thpo*, which single-handedly caused the entire phenotype. The trajectory of this project has been beyond our expectations, and we present our findings to the platelet and megakaryocyte community in the hopes that the results may be of use or interest.

Conclusions

- A single-base pair, single-amino acid change in the EPO-like domain of TPO leads to altered protein conformation, impaired TPO-Mpl binding, and a post-translational loss of TPO protein.
- The *C57Bl/6 (IMPC)J-TPO*^{L121H} mouse strain is characterized by a ~ 95% loss of circulating TPO protein but preserved TPO mRNA, making it suitable for the study of thrombocytopenia of intermediate severity and of transcriptional TPO regulation.
- The identification of a novel mechanism of TPO deficiency raises the possibility of rare clinical thrombocytopenia syndromes that may be mediated through post-transcriptional mechanisms.

Acknowledgments

We would like to thank Mihaela Gadjeva, who provided the original PCYOX1L knockout mouse model as well as Mark Distefano, who taught us about the importance of protein prenylation. Thank you to Michael Sykes and Brian Sykes who helped with the protein structure modeling and predictions. Thank you to Vijay Sankaran who examined human thrombopoietin across the whole exome sequencing databases. Thank you to Steve Murray of Jackson laboratories for providing the original mouse phenotyping data and aiding in early troubleshooting experiments. Thank you to Maris Handley and our colleagues within the Center for Regenerative Medicine flow cytometry core. Thank you to Anna Berling and Hanna Tegel at the KTH Royal Institute of Technology for synthesis and troubleshooting of the recombinant TPO proteins. Thank you to Jelena Milosevic, Nathan Jeffries, Adena Pepich, Kristina Ihrmark-Lundberg, Ioanna Tsea, Celine Hafkesbrink, and Emmi Puuvuori for their help and support in the lab.

Disclosure statement

No potential conflict of interest was reported by the author(s).

References

1. Kuter DJ. The biology of thrombopoietin and thrombopoietin receptor agonists. Int J Hematol. 2013;98(1):10–23. doi: 10.1007/s12185-013-1382-0.
2. Hitchcock IS, Kaushansky K. Thrombopoietin from beginning to end. Br J Haematol. 2014;165(2):259–268. doi: 10.1111/bjh.12772.
3. Graaf CD, Metcalf D. Thrombopoietin and hematopoietic stem cells. Cell Cycle. 2011;10(10):1582–1589. doi: 10.4161/cc.10.10.15619.
4. Murone M, Carpenter DA, Sauvage FD. Hematopoietic deficiencies in c-mpl and TPO knockout mice. STEM Cells. 1998;16(1):1–6. doi: 10.1002/stem.160001.
5. Sungaran R, Markovic B, Chong BH. Localization and regulation of thrombopoietin mRNA expression in human kidney, liver, bone marrow, and spleen using in situ hybridization. Blood. 1997;89(1):101–107. doi: 10.1182/blood.V89.1.101.
6. Kuter DJ. The physiology of platelet production. STEM Cells. 1996;14(S1):88–101. doi: 10.1002/stem.5530140711.
7. Peck-Radosavljevic M. Thrombocytopenia in chronic liver disease. Liver Int. 2017;37(6):778–793. doi: 10.1111/liv.13317.
8. Li J, Yang C, Xia Y, Bertino A, Glaspy J, Roberts M, Kuter DJ. Thrombocytopenia caused by the development of antibodies to thrombopoietin. Blood. 2001;98(12):3241–3248. doi: 10.1182/blood.V98.12.3241.

9. Hirata S, Takayama N, Jono-Ohnishi R, Endo H, Nakamura S, Dohda T, Nishi M, Hamazaki Y, Ishii E-I, Kaneko S, et al. Congenital amegakaryocytic thrombocytopenia iPS cells exhibit defective MPL-mediated signaling. J Clin Investig. 2013;123(9):3802–3814. doi: 10.1172/JCI64721.
10. Bussel JB, Provan D, Shamsi T, Cheng G, Psaila B, Kovaleva L, Salama A, Jenkins JM, Roychowdhury D, Mayer B, et al. Effect of eltrombopag on platelet counts and bleeding during treatment of chronic idiopathic thrombocytopenic purpura: a randomised, double-blind, placebo-controlled trial. Lancet. 2009;373 (9664):641–648. doi: 10.1016/S0140-6736(09)60402-5.
11. Alexander WS, Roberts AW, Nicola NA, Li R, Metcalf D. Deficiencies in progenitor cells of multiple hematopoietic lineages and defective megakaryocytopoiesis in mice lacking the thrombopoietic receptor c-Mpl. Blood. 1996;87(6):2162–2170. doi: 10.1182/blood.V87.6.2162.bloodjournal8762162.
12. Sauvage FD, Carver-Moore K, Luoh SM, Ryan A, Dowd M, Eaton DL, Moore MW. Physiological regulation of early and late stages of megakaryocytopoiesis by thrombopoietin. J Exp Med. 1996;183(2):651–656. doi: 10.1084/jem.183.2.651.
13. Gurney A, Carver-Moore K, Sauvage FD, Moore M. Thrombocytopenia in c-mpl-deficient mice. Science. 1994;265(5177):1445–1447. doi: 10.1126/science.8073287.
14. Nakamura-Ishizu A, Chin DWL, Matsumura T, Tan DQ, Mochizuki-Kashio M, Jianwen D, Suda T. Prolonged maintenance of hematopoietic stem cells that escape from thrombopoietin deprivation. Blood. 2021;137 (19):2609–2620. doi: 10.1182/blood.2020005517.
15. Decker M, Leslie J, Liu Q, Ding L. Hepatic thrombopoietin is required for bone marrow hematopoietic stem cell maintenance. Science. 2018;360(6384):106–110. doi: 10.1126/science.aap8861.
16. Shirai T, Revenko AS, Tibbitts J, Ngo ATP, Mitrugno A, Healy LD, Johnson J, Tucker EI, Hinds MT, Coussens LM, et al. Hepatic thrombopoietin gene silencing reduces platelet count and breast cancer progression in transgenic MMTV-PyMT mice. Blood Adv. 2019;3(20):3080–3091. doi: 10.1182/bloodadvances.2019000250.
17. Barrett TJ, Wu BG, Revenko AS, MacLeod AR, Segal LN, Berger JS. Antisense oligonucleotide targeting of thrombopoietin represents a novel platelet depletion method to assess the immunomodulatory role of platelets. J Thromb Haemost. 2020;18(7):1773–1782. doi: 10.1111/jth.14808.
18. Yang L, Wu L, Meng P, Zhang X, Zhao D, Lin Q, Zhang Y. Generation of a thrombopoietin-deficient thrombocytopenia model in zebrafish. J Thromb Haemost. 2022;20(8):1900–1909. doi: 10.1111/jth.15772.
19. Grozovsky R, Begonja AJ, Liu K, Visner G, Hartwig JH, Falet H, Hoffmeister KM. The Ashwell-Morell receptor regulates hepatic thrombopoietin production via JAK2-STAT3 signaling. Nat Med. 2015;21(1):47–54. doi: 10.1038/nm.3770.
20. McIntosh B, Kaushansky K. Transcriptional regulation of bone marrow thrombopoietin by platelet proteins. Exp Hematol. 2008;36(7):799–806. doi: 10.1016/j.exphem.2008.02.012.
21. Kaser A, Brandacher G, Steurer W, Kaser S, Offner FA, Zoller H, Theurl I, Widder W, Molnar C, Ludwiczek O, et al. Interleukin-6 stimulates thrombopoiesis through thrombopoietin: role in inflammatory thrombocytosis. Blood. 2001;98(9):2720–2725. doi: 10.1182/blood.V98.9.2720.
22. Kawasaki T, Takeshita A, Souda K, Kobayashi Y, Kikuyama M, Suzuki F, Kageyama F, Sasada Y, Shimizu E, Murohisa G, et al. Serum thrombopoietin levels in patients with chronic hepatitis and liver cirrhosis. Am J Gastroenterol. 1999;94(7):1918–1922. doi: 10.1111/j.1572-0241.1999.01231.x.
23. Koruk M, Onuk MD, Akçay F, Savas MC. Serum thrombopoietin levels in patients with chronic hepatitis and liver cirrhosis, and its relationship with circulating thrombocyte counts. Hepato-Gastroenterol. 2002;49 (48):1645–1648.
24. Gurney AL, Kuang WJ, Xie MH, Malloy BE, Eaton DL, Sauvage FD. Genomic structure, chromosomal localization, and conserved alternative splice forms of thrombopoietin. Blood. 1995;85(4):981–988. doi: 10.1182/blood.V85.4.981.bloodjournal854981.
25. Mercier FE, Sykes DB, Scadden DT. Single targeted exon mutation creates a true congenic mouse for competitive hematopoietic stem cell transplantation: the C57BL/6-CD45.1STEM mouse. STEM Cell Rep. 2016;6(6):985–992. doi: 10.1016/j.stemcr.2016.04.010.
26. Hoggatt J, Singh P, Sampath J, Pelus LM. Prostaglandin e2 enhances hematopoietic stem cell homing, survival, and proliferation. Blood. 2009;113(22):5444–5455. doi: 10.1182/blood-2009-01-201335.
27. He XC, Li Z, Sugimura R, Ross J, Zhao M, Li L. Hematopoietic stem cell protocols. Methods Mol Biol. 2014;1185:279–284.
28. Lapidot T, Dar A, Kollet O. How do stem cells find their way home? Blood. 2005;106(6):1901–1910. doi: 10.1182/blood-2005-04-1417.
29. Chen S, Francioli LC, Goodrich JK, Collins RL, Kanai M, Wang Q, Alföldi J, Watts NA, Vittal C, Gauthier LD, et al. A genome-wide mutational constraint map quantified from variation in 76,156 human genomes. BioRxiv. 2022;2022.03.20.485034.
30. Sayers EW, Bolton EE, Brister JR, Canese K, Chan J, Comeau DC, Farrell CM, Feldgarden M, Fine AM, Funk K, et al. Database resources of the National Center for Biotechnology Information in 2023. Nucleic Acids Res. 2022;51(D1):gkac1032–.
31. Mirdita M, Schütze K, Moriwaki Y, Heo L, Ovchinnikov S, Steinegger M. ColabFold: making protein folding accessible to all. Nat Methods. 2022;19(6):679–682. doi: 10.1038/s41592-022-01488-1.

32. Pettersen EF, Goddard TD, Huang CC, Couch GS, Greenblatt DM, Meng EC, Ferrin TE. Ucsf Chimera—a visualization system for exploratory research and analysis. J Comput Chem. 2004;25(13):1605–1612. doi: 10.1002/jcc.20084.
33. Haase C, Gustafsson K, Mei S, Yeh SC, Richter D, Milosevic J, Turcotte R, Kharchenko PV, Sykes DB, Scadden DT, et al. Image-seq: Spatially resolved single-cell sequencing guided by in situ and in vivo imaging. Nat Methods. 2021;19(12):1622–1633. doi: 10.1038/s41592-022-01673-2.
34. Barkas N, Petukhov V, Nikolaeva D, Lozinsky Y, Demharter S, Khodosevich K, Kharchenko PV. Joint analysis of heterogeneous single-cell RNA-seq dataset collections. Nat Methods. 2019;16(8):695–698. doi: 10.1038/s41592-019-0466-z.
35. Tegel H, Dannemeyer M, Kanje S, Sivertsson Å, Berling A, Svensson AS, Hober A, Enstedt H, Volk A-L, Lundqvist M, et al. High throughput generation of a resource of the human secretome in mammalian cells. N Biotechnol. 2020;58:45–54. doi: 10.1016/j.nbt.2020.05.002.
36. Beigneux A, Withycombe SK, Digits JA, Tschantz William R, Weinbaum CA, Griffey SM, Bergo M, Casey PJ, Young SG. Prenylcysteine lyase deficiency in mice results in the accumulation of farnesylcysteine and geranylgeranylcysteine in brain and liver*. J Biol Chem. 2002;277(41):38358–38363. doi: 10.1074/jbc.M205183200.
37. Petenkova A, Auger SA, Lamb J, Quellier D, Carter C, To OT, Milosevic J, Barghout R, Kugadas A, Lu X, et al. Prenylcysteine oxidase 1 like protein is required for neutrophil bactericidal activities. Nat Commun. 2023;14(1):2761. doi: 10.1038/s41467-023-38447-z.
38. Sauvage FJD, Villeval JL, Shivdasani RA. Regulation of megakaryocytopoiesis and platelet production: lessons from animal models. J Lab Clin Med. 1998;131(6):496–501. doi: 10.1016/S0022-2143(98)90057-9.
39. Morowski M, Vögtle T, Kraft P, Kleinschnitz C, Stoll G, Nieswandt B. Only severe thrombocytopenia results in bleeding and defective thrombus formation in mice. Blood. 2013;121(24):4938–4947. doi: 10.1182/blood-2012-10-461459.
40. Bunting S, Widmer R, Lipari T, Rangell L, Steinmetz H, Carver-Moore K, Moore MW, Keller G-A, de Sauvage FJ. Normal platelets and megakaryocytes are produced in vivo in the absence of thrombopoietin. Blood. 1997;90(9):3423–3429. doi: 10.1182/blood.V90.9.3423.
41. O'Neill A, Chin D, Tan D, Majeed AQBBA, Nakamura-Ishizu A, Suda T. Thrombopoietin maintains cell numbers of hematopoietic stem and progenitor cells with megakaryopoietic potential. Haematologica. 2020;106(7):1883–1891. doi: 10.3324/haematol.2019.241406.
42. Lee Y, DiMaulo-Milk E, Leslie J, Ding L. Hematopoietic stem cells temporally transition to thrombopoietin dependence in the fetal liver. Sci Adv. 2022;8(11):eabm7688. doi: 10.1126/sciadv.abm7688.
43. Kaushansky K. Thrombopoietin, the primary regulator of platelet production: from mythos to logos, a thirty-year journey. Biomolecules. 2024;14(4):489. doi: 10.3390/biom14040489.
44. Dasouki MJ, Rafi SK, Olm-Shipman AJ, Wilson NR, Abhyankar S, Ganter B, Furness LM, Fang J, Calado RT, Saadi I. Exome sequencing reveals a thrombopoietin ligand mutation in a Micronesian family with autosomal recessive aplastic anemia. Blood. 2013;122(20):3440–3449. doi: 10.1182/blood-2012-12-473538.
45. Cohen-Solal K, Villeval JL, Titeux M, Lok S, Vainchenker W, Wendling F. Constitutive expression of MPL ligand transcripts during thrombocytopenia or thrombocytosis. Blood. 1996;88(7):2578–2584. doi: 10.1182/blood.V88.7.2578.bloodjournal8872578.
46. Stoffel R, Wiestner A, Skoda R. Thrombopoietin in thrombocytopenic mice: evidence against regulation at the mRNA level and for a direct regulatory role of platelets. Blood. 1996;87(2):567–573. doi: 10.1182/blood.V87.2.567.bloodjournal872567.
47. Yang C, Li YC, Kuter DJ. The physiological response of thrombopoietin (c-Mpl ligand) to thrombocytopenia in the rat. Br J Haematol. 1999;105(2):478–485. doi: 10.1111/j.1365-2141.1999.01359.x.
48. Wolber EM, Jelkmann W. Interleukin-6 increases thrombopoietin production in human hepatoma cells HepG2 and Hep3B. J Interf Cytokine Res. 2000;20(5):499–506. doi: 10.1089/10799900050023915.
49. Stone RL, Nick AM, McNeish IA, Balkwill F, Han HD, Bottsford-Miller J, Rupairmoole R, Armaiz-Pena GN, Pecot CV, Coward J, et al. Paraneoplastic thrombocytosis in ovarian cancer. N Engl J Med. 2012;366(7):610–618. doi: 10.1056/NEJMoa1110352.
50. McCarty JM, Sprugel KH, Fox NE, Sabath DE, Kaushansky K. Murine thrombopoietin mRNA levels are modulated by platelet count. Blood. 1995;86(10):3668–3675. doi: 10.1182/blood.V86.10.3668.bloodjournal86103668.
51. Sungaran R, Chisholm OT, Markovic B, Khachigian LM, Tanaka Y, Chong BH. The role of platelet alpha-granular proteins in the regulation of thrombopoietin messenger RNA expression in human bone marrow stromal cells. Blood. 2000;95(10):3094–3101.
52. Kinjo K, Miyakawa Y, Uchida H, Kitajima S, Ikeda Y, Kizaki M. All-trans retinoic acid directly up-regulates thrombopoietin transcription in human bone marrow stromal cells. Exp Hematol. 2004;32(1):45–51. doi: 10.1016/j.exphem.2003.10.009.
53. Wu D, Xie J, Wang X, Zou B, Yu Y, Jing T, Zhang S, Zhang Q. Micro-concentration lipopolysaccharide as a novel stimulator of megakaryocytopoiesis that synergizes with IL-6 for platelet production. Sci Rep. 2015;5(1):13748. doi: 10.1038/srep13748.

54. Kanagasabapathy D, Blosser RJ, Maupin KA, Hong JM, Alvarez M, Ghosh J, Mohamad SF, Aguilar-Perez A, Srour EF, Kacena MA, et al. Megakaryocytes promote osteoclastogenesis in aging. Aging (Albany NY). 2020;12 (14):15121–15133. doi: 10.18632/aging.103595.
55. Tucker EI, Marzec UM, Berny MA, Hurst S, Bunting S, McCarty OJT, Gruber A, Hanson SR. Safety and antithrombotic efficacy of moderate platelet count reduction by thrombopoietin inhibition in primates. Sci Transl Med. 2010;2(37):37ra45. doi: 10.1126/scitranslmed.3000697.
56. Yoshihara H, Arai F, Hosokawa K, Hagiwara T, Takubo K, Nakamura Y, Gomei Y, Iwasaki H, Matsuoka S, Miyamoto K, et al. Thrombopoietin/MPL signaling regulates hematopoietic stem cell quiescence and interaction with the osteoblastic niche. Cell Stem Cell. 2007;1(6):685–697. doi: 10.1016/j.stem.2007.10.020.
57. Gotoh A, Ritchie A, Takahira H, Broxmeyer HE. Thrombopoietin and erythropoietin activate inside-out signaling of integrin and enhance adhesion to immobilized fibronectin in human growth-factor-dependent hematopoietic cells. Ann Hematol. 1997;75(5–6):207–213. doi: 10.1007/s002770050344.
58. Liu Y, Ding L, Zhang B, Deng Z, Han Y, Wang S, Yang S, Fan Z, Zhang J, Yan H, et al. Thrombopoietin enhances hematopoietic stem and progenitor cell homing by impeding matrix metalloproteinase 9 expression. STEM CELLS Transl Med. 2020;9(6):661–673. doi: 10.1002/sctm.19-0220.
59. Kaushansky K, Broudy VC, Grossmann A, Humes J, Lin N, Ren HP, Bailey MC, Papayannopoulou T, Forstrom JW, Sprugel KH. Thrombopoietin expands erythroid progenitors, increases red cell production, and enhances erythroid recovery after myelosuppressive therapy. J Clin Investig. 1995;96(3):1683–1687. doi: 10.1172/JCI118210.